The green combustion technique for synthesizing CuO nanoparticles with an extract from *Azadirachta indica* seeds: potential anticancer and photocatalytic studies using organic dye

P. Kalaivani [a], G. Mathubala [b,*]
[a] *Research Scholar, Department of Chemistry, Bharath Institute of Higher Education and Research, BIST, Chennai-73, Tamil Nadu, India.*
[b*] *Professor and Head, Department of Chemistry, Bharath Institute of Higher Education and Research, BIST, Chennai-73, Tamil Nadu, India.*

The present study highlights the biosynthesis of CuO nanoparticles employing an *A. indica* seed extract and copper sulphate solution by combustion technique. The extract's phytocomponents facilitated the reduction process and the formation of copper oxide nanoparticles (CuONPs). TEM, SEM, FTIR, X-ray diffractometry, XPS, and ultraviolet-visible spectroscopy were used to analyse the pure CuONPs. X-ray diffractometers characterized the CuONPs produced, demonstrating a 12 nm mean particle size. Cu-O stretching vibration bands were detected at 532 cm^{-1} in the FT-IR spectrum. In UV-vis, the CuO nanoparticles' optical band gaps were at 2.75 eV, with a maximum absorption wavelength of 232 nm. SEM and HRTEM were used to examine the CuONPs; they displayed spherical and undefined shapes with mean sizes of 17.4 nm. The pollution dye rhodamine B was used to test the CuONPs photocatalytic activity. In the presence of sunlight, a remarkable 85% degradation efficiency was attained in 60 minutes, and a degradation constant of k (0.9194 min^{-1}) was observed. This suggests that *Azardirachta indica* seed extract-derived green-synthesized CuONPs have potential uses in photocatalysis. Furthermore, in the MTT assay method against human renal adenocarcinoma cancer cells, the CuO NPs showed strong anticancer activity, with 5 mg/mL as the lowest IC50 value. This novel green method has demonstrated copper oxide nanoparticle synthesis is a very successful and cost-effective pollutant adsorption technique for treating wastewater.

(Received September 26, 2024; Accepted January 13, 2025)

Keywords: Copper oxide nanoparticles, Azardirachta indica, HRTEM, HRSEM

1. Introduction

The unique electrical, optical, and catalytic qualities of single-spatial semiconductor nanoparticles make them potentially useful in many different fields. Among these are electronics, photovoltaic applications, energy storage, and catalysis [1]. The potential of semiconductor photocatalysts to provide transparent mechanisms with light-based chemical transformation capabilities has drawn a considerable amount of interest. Light entering a semiconductor causes electrons to travel in the direction of the conduction band, departing the valence holes and electrons behind them as they absorb the photons' energy [2]. Synthesized e- and h+ couples start dye-degradation activities on the semiconductor surface. Metal oxides with different band gaps are the most common type of photocatalyst used in environmental clean-up. About 4% of the spectrum's solar energy can be absorbed by a semiconductor with a large band gap [3]. Thus solar energy, which is cheap, abundant, and rarely runs out, is the subject of continuous research [4,5]. The researchers are interested in visible-light photocatalysts because of their potential applications in energy and the environment. Pairing energetic electrons and holes created during recombination could limit the semiconductor's ability to catalyse photosynthesis [6,7]. Therefore, creating catalysts powered by

* Corresponding author: kalaivanipolur94@gmail.com
https://doi.org/10.15251/DJNB.2025.201.37

visible light is a difficult task. Green nanotechnology is cantered on creating nanomaterials using non-toxic substances in gentle processing settings, which increases the nanoparticles' environmental sustainability [8]. The biogenic synthesis, often known as the "green synthesis approach," offers an appropriate framework for the environmentally responsible and sustainable production of nanomaterials. Plant and microbe mediated biogenic synthesis are the two primary methods to produce nanomaterials. Both these methods are growing in popularity due to their greater accessibility, being less expensive, and involve a simpler process [9]. When it comes to semiconductors, their moderate band gap, and simultaneous performance, or support of oxidation and reduction, are their unique characteristics. Free electron-hole pairs are created when light falls. A low recombination rate is a prerequisite for a semiconductor to function as a photocatalyst. Additionally, semiconductors that have a visible band gap (1.5-3.5 eV) or an absorption wavelength (350-700 nm) are appropriate for photocatalytic activity, since they exhibit catalytic activity when exposed to light (10). Creating techniques for disintegrating dyes is difficult for researchers [11, 12]. Chemical oxidation, ion exchange, photocatalytic degradation, ozonolysis, and coagulation-based approaches are a few of these processes [13, 14]. Using a semiconductor photocatalyst to degrade dyes is expected to be a cost-effective and environmentally friendly solution [15, 16, 17]. Thus treating wastewater before releasing it into water bodies is crucial. Since xanthene dyes like rhodamine B (RhB) are widely used in industry, they were chosen for this study's model pollutant. Because of its low capacity for deterioration and great stability, it has an impact on the aquatic system [(18)]. India is a tropical nation where photocatalysts can be exposed to an abundance of sunlight. The degradation of the dyes is fuelled by visible light [19]. To break down organic dyes, light-active substances with a more surface area is required [20]. A modest band gap in several metal oxides and semiconductors makes them active photocatalysts in the presence of sunlight [21]. CuO exhibits a 2.1 to 2.71 eV band gap, making it a p-type semiconductor. Applications involving optics, mechanics, and photolysis respond well to CuO nanoparticles (NPs) [22]. Several techniques, such as solvothermal, sol-gel, hydrothermal, microwave irradiation, arc discharge, etc., are used to create CuO NPs [23]. CuONPs were therefore discovered to be more advantageous than noble metals in plasmonic catalysis because of their inexpensive cost. Over a broad range of wavelength spectra, it can demonstrate good LSPR properties. Apart from its remarkable stability during photocatalysis, it has demonstrated the ability of oxygen (O_2) and water (H_2O) molecules to oxidise CuONPs [24]. Phenolic chemicals, flavonoids, quinol, terpenoids, alkaloids, and chlorophyll pigments all contribute significantly to the chemical makeup of plants and can reduce metal ions [25]. The most feasible and environment friendly method is thought to be the production of CuO NPs using plant extracts [26]. CuONPs can be produced by different biogenic techniques, such as using fungi, plants, algae, and bacteria as biologically active components by extracting active ingredient from their flowers, leaves, or stems, such as betel leaf, [27] Seriphidium oliverianum, [28] Catha edulis, [29] Cinchona bark, [30] Macrocystis pyrifera, [31] Cinnamomum malabatrum, etc. [32]. Numerous attempts were undertaken to comprehend the properties of CuONPs and their biological mechanisms, as well as the phytochemicals involved in their green production [33]. A variety of biomolecules, including vitamins, alkaloids, polysaccharides, proteins and enzymes, alcoholic chemicals, and amino acids, can stabilise nanoparticles [34]. Plants that contain biological substances such as enzymes and polyphenols, among other chelating agents, have varying levels of reducing power, that affects the generated CuONPs [35].

Neem has an abundance of different kinds of components that make it a therapeutic choice for managing health. The principal active component is azadirachtin; other components are quercetin, gedunin, salannin, sodium nimbinate, nimbin, nimbidin, and nimbidol. Seeds have beneficial components such as azadirachtin and gedunin. Neem's abundance of antioxidants contributes to its ability to scavenge free radicals. The following was the sequence in which nimbolide and azadirachtin demonstrated concentration-dependent reductive potential and antiradical scavenging activity: Azadirachtin > nimbolide > ascorbate. The active ingredient in neem has shown to effectively manage cancer by regulating cell signalling pathways. Neem interacts with several tumour suppressor genes, including p53 and pTEN, as well as transcription factors, angiogenesis (VEGF), apoptosis (bcl2, bax) etc. Neem also reduces inflammation by preventing pro-inflammatory enzymes such as lipoxygenase and cyclooxygenase from acting [36]. When CuO nanoparticles are formed, the metabolites can function as a complexing and capping agent [37]. In

this study, the green synthesis of CuONPs using a reducing agent is sourced from the seed extract of *Azardirachta indica*. Following this, FTIR, X-ray diffractometry, UV-vis, HRSEM, XPS, and HRTEM were used to analyse the CuONPs. The capacity of the green-produced CuONPs to catalyse RhB dye under solar light irradiation was investigated.

2. Experimental

2.1. Materials and methods

2.1.1. Chemicals

The seedlings of *A. indica* were procured from a nearby garden in Chennai, Tamil Nadu, India. RB dye, copper(II) sulphate pentahydrate CuSO4·5H2O, was acquired from Sigma Aldrich (St. Louis, MO, USA). All investigations were conducted with deionized (DI) water. Unless otherwise specified, all other chemicals were of analytical grade.

2.1.2. Plant extract

A magnetic stirrer was used to mix 300 ml of distilled water with 30 grams of thoroughly cleaned *A. indica* dry seed. Subsequently, the blend was placed on a heated plate and allowed to boil at 80 °C for two hours. An uncontaminated aqueous extract was produced by allowing the seed extract to reach room temperature and then filtering it three times with Whatman No.1 filter paper. A pH of 7.3 was used to assess the aqueous extract, which is regarded as neutral at room temperature. The seed extract refrigerated at 4 °C was used for our study. This is shown in Fig 1.

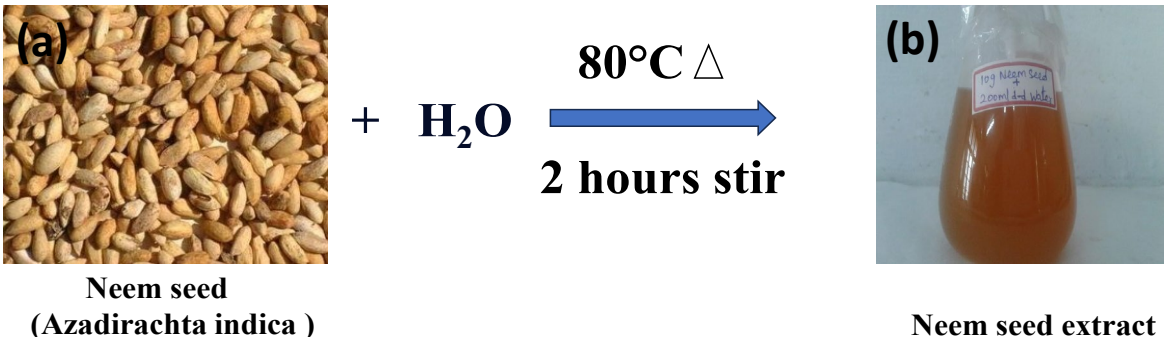

Fig. 1. (a-b). Preparation of seed extract: a) mixture of dry neem seed and deionized water; b) preparation of an extract from neem seed.

2.1.3. Copper oxide nanoparticle synthesis

Copper sulphate solution and *A. indica* seed extract was boiled on a hot plate to create CuONPs. A clear and homogenous mixture was obtained after combining 80 ml of an aqueous solution containing 1 mM CuSO4.5H2O with 20 ml of plant extract and stirring the mixture for an hour. Over a hot plate, it took fifteen minutes to bring the resultant mixture up to 50 °C. The deep brown colour powder was obtained by boiling, then drying at 110 °C in a hot air oven. After two hours of annealing at 300 °C, one gram of copper oxide by weight was produced from the dark brown powdered CuONPs. This is depicted in Fig 2.

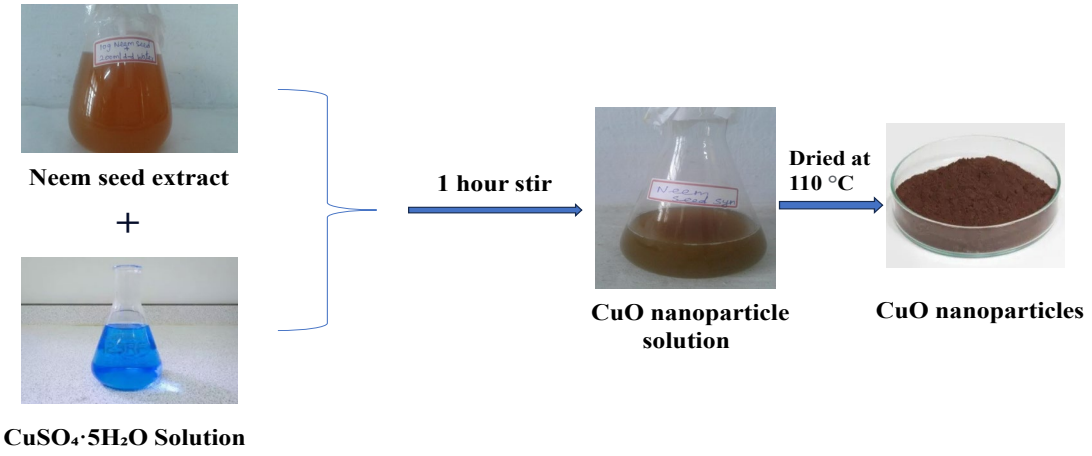

Fig. 2. CuONPs Synthesising process: Colour change was observed during the reduction of $CuSO_4.5H_2O$ to CuONPs from neem seed extract.

The primary constituents of neem seeds are azadirachtin and gedunin. These phytonutrients functions as capping agents to convert copper ions into nanoparticles and are crucial to the bio-reduction process. Regarding copper oxide, numerous studies have been published on the biosynthesis of nanomaterials using polyphenolic chemicals as environmentally friendly reductants [38]. *A. indica* seed extract is a potent source of flavonoid and polyphenolic components. The significant function of these phytonutrients is to act as a reductant for CuONPs formation. Fig 3 illustrates a potential route for producing CuONPs using a green combustion synthesis method. When the aqueous extract of *A. indica* seed and copper sulphate solution are mixed, a polyphenolic complex containing Cu2+ ions are initially formed. When the reduction is complete, CuONPs are produced. Stable CuONPs are formed when the Cu atoms continue oxidising in ambient oxygen. When copper oxide nanoparticles crystallize, isolable materials grow faster.

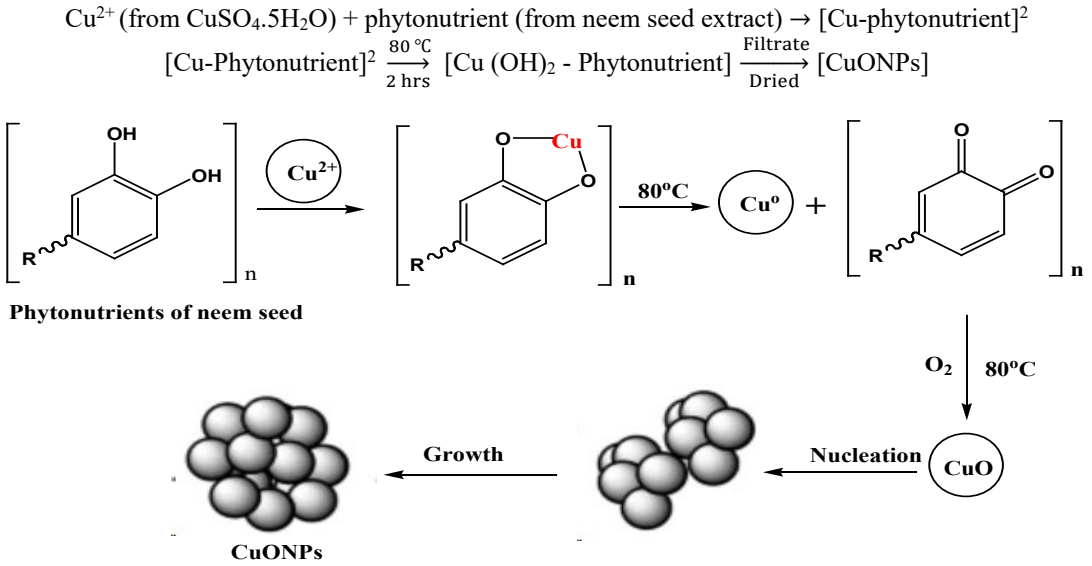

Fig. 3. Mechanism of CuO nanoparticle formation.

2.1.4. Characterization of copper oxide nanoparticles

The CuONPs were analysed with an HRTEM (JEOL Japan, JEM-2100 Plus) and the sizes of the nanoparticles were determined using the Image J software after they were randomly selected

from HRTEM images. TEM and HRSEM were used to analyse the copper oxide nanoparticles' topography, size, and morphology. CuONPs phase formation and crystal structure were investigated by powder XRD using a 2.2 KW Cu anode in a Ceramic X-ray tube (Bruker, D8 Advance). The prepared material's molecular structure and functional groups were determined by FT-IR analysis (PERKIN ELMER RX-1). Using scanning electron microscopy, the material's morphology and microstructure were identified using SEM (JEOL JSM 5600). CuONPs, measuring between 350 and 500 nm in size, were examined using UV-vis spectroscopy at JASCO (V-670 PC). The XPS device can determine the elemental composition as well as the chemical and electronic states of atoms within a substance. XPS was analysed with a (PHI-Versa Probe 4) after they were formed.

2.1.5. Photodegradation studies

The generated sample's rate of photocatalytic degradation ability was tested against rhodamine B (RB) when UV light was applied to CuONPs. To achieve a 2 x 10^{-5} M concentration of RB dye, 20 ml of the RB dye was dissolved in 100 ml of deionized water (H2O), and 20 mg of CuONPs catalyst was added to the RB dye solution. To determine the RB dye solution's degradation potential, the catalyst-containing dye solution with CuONPs was placed in a 500-watt xenon lamp photo reactor and exposed to UV radiation. The dye degradation in the aqueous solution was monitored every 10 minutes. The effective degradation percentage was determined by performing the following equation:

$$Degradation\ efficiency\ (\%) = \frac{Initial\ absorbance - Final\ absorbance}{Initial\ absorbance}\ X\ 100\ \% \quad (1)$$

2.1.6. Anticancer analysis

The anticancer effect of the *A. indica* seed extract was examined by treating Ehrlich Ascites Carcinoma and HT-29 cells for 24 hours. The cells' vitality was then verified using the MTT test. A 24-hour incubation period was allowed for the cells to become 60% confluent before they were trypsinised in 96-well plates. 9000 cells were placed in each well. Following a 24-hour incubation period, various concentrations of *A. indica* seed extract and CuONPs were applied. The cells were washed with phosphate-buffered saline after discarding the medium, and 20 ml of MTT reagent was added to each well. The wells were then placed in a water bath set to 37 °C for four hours. Subsequently, 200 ml of acidic isopropanol was added, and the plate shaker was left in the dark for 30 minutes. To dissolve the crystals, we employed 100 ml of dimethyl sulfoxide. The percentage of live cells was estimated by measuring the absorbance at 570 nm, and the anticancer effect was inferred from there.

3. Results and discussion

3.1. Structural analysis

The crystalline structure of CuONPs made from *A. indica* seed extract was verified through X-ray diffractometry [39], Fig 4. The XRD patterns revealed the diffractogram showing the primary strong angles of the green synthesis of CuONPs, proving the crystallographic character. The CuONPs were crystalline and found on JCPDS Card No. 04-0835 in the fcc cubic structure, as seen by strong peaks in the X-ray diffractometry patterns. All the peaks that were designated for the planes were in order of 37.19 º (222), 43.26 º (311), 62.99 º (200), 75.55 º (220), and 79.23 º (111) [40]. No reflection was associated with any impurity till the XRD diffractometer's detection limit which was confirmed in the XRD pattern, further demonstrating the purity of the CuONPs. Furthermore, the high intensity and well-defined diffraction reflections obtained provide strong evidence for the biosynthesis of CuO NP's well-crystalline structure. Using the Debye-Scherrer formula (1), the nanoparticle size was determined and could be expressed as

$$D = \frac{K\lambda}{\beta \cos\theta} \quad (2)$$

The computation results were presented in the preceding equation. The average size of the crystal for the green combustion method of CuONPs synthesis has been observed at 12 nm, based on the well-known Scherrer equation (2). In this case, the wavelength at which Cu Kα produces X-rays is 1.5405 Å, or λ, and the constant k has a value of 0.9. The XRD pattern's intensity peak's 2θ value calculates the Bragg angle, or θ. The symbol β represents the whole breadth at half of the maximum diffraction of the green-produced CuO nanoparticles [41]. Consequently, the outcomes back up the formation of CuO nanoparticles. There are no other contaminants visible in the CuONPs diffractogram.

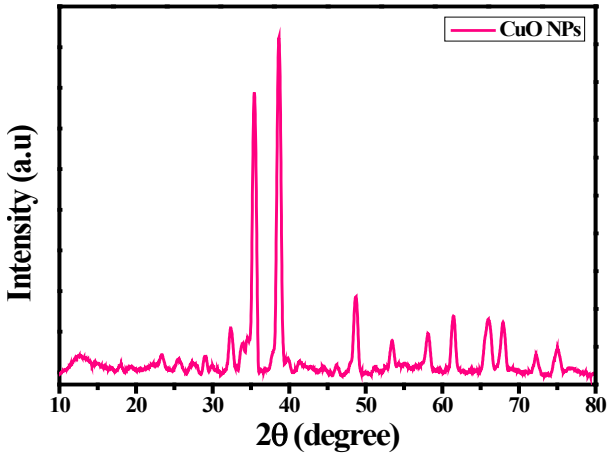

Fig. 4. XRD spectrum of the green combustion method of copper oxide nanoparticle synthesis from Neem seed extract.

3.2. Functional group analysis

FTIR spectra were used to identify the functional group of *A. indica* seed extract and CuONPs. This is shown in Fig 5 (a, b). The Cu-O vibration mode is widespread between 400 and 600 cm^{-1} [42]. O-H bending of the phenolic group was demonstrated by the peak at 1463 cm^{-1} for the seed extract of *A. indica*, the shifted band were at 1392 cm^{-1} for CuONPs, and band peaking at around 613 cm^{-1}. The absorption peak at 1240 cm^{-1} of the C-O stretching vibration bond was seen in the *A. indica* seed extract spectrum, whereas for CuONPs, it was at a displaced peak at 1102 cm^{-1}. The presence of primary amide groups was verified by absorption bands at 1639 and 1632 cm^{-1} for *A. indica* seed extract and CuONPs, respectively.

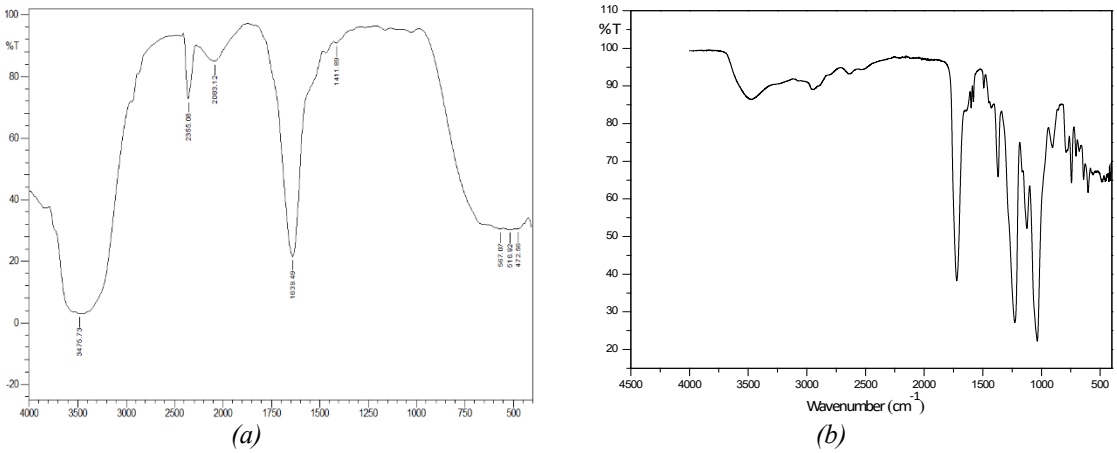

(a) *(b)*

Fig. 5(a-b). FT-IR results of a) seed extract of A. indica, b) green synthesis combustion method of CuO nanoparticles from A. indica seed extract.

The presence of primary amide produced from the protein content of *A. indica* seeds further revealed that the protein in the seeds served as a reducing and capping agents during the formation of CuONPs. The CuONPs O-H stretching vibration bond was shown by the absorption peaks at 3475 and 3390 cm^{-1} in the *A. indica* seed extract. The CuONPs did not exhibit C-H stretching in the seed extract (2355 cm^{-1}). The CuONPs stretching vibration of Cu-O caused a significant and strong absorption peak at 532 cm^{-1} and was absent in the seed [43].

3.3. UV-visible spectrum analysis

Green-produced CuONPs with wavelengths between 300 and 800 nm were investigated using their UV-visible spectra Fig 6(a). The charge transfers between the VB and CB caused by the cation accounts for the ultraviolet-visible spectra of the formation of CuONPs at 232 nm. The reaction mixture's brown colouration was due to the copper oxide particles' surface plasmon oscillations. The formation of CuONPs is shown by this colour shift. Using a UV-vis spectrophotometer, a spectrum analysis examination was conducted to investigate the reduction of copper sulphate. As a result, 232 nm was the reported absorption peak for the green-produced CuO NPs [44]. The spectrum showed that when the particle gets closer to signals with successively shorter wavelengths, its size decreases. As a result, it was found that the formation of oxides involving functional groups produced metal nucleation. The Kubelka-Munk relation can be used to calculate the E_G of CuONPs. The CuONPs produced by green synthesis have an E_G of 2.75 eV [45], Fig 6(b). The CuONPs optical band gap strongly affects photocatalytic activity which can be predicted using the optical band gap. An optical band gap below 5 eV is better for CuONPs photocatalytic action. The following Tauc formula is used to determine the CuO nanoparticle's optical band gap (3).

$$(\alpha h\nu)\, n = A\,(h\nu - Eg) \tag{3}$$

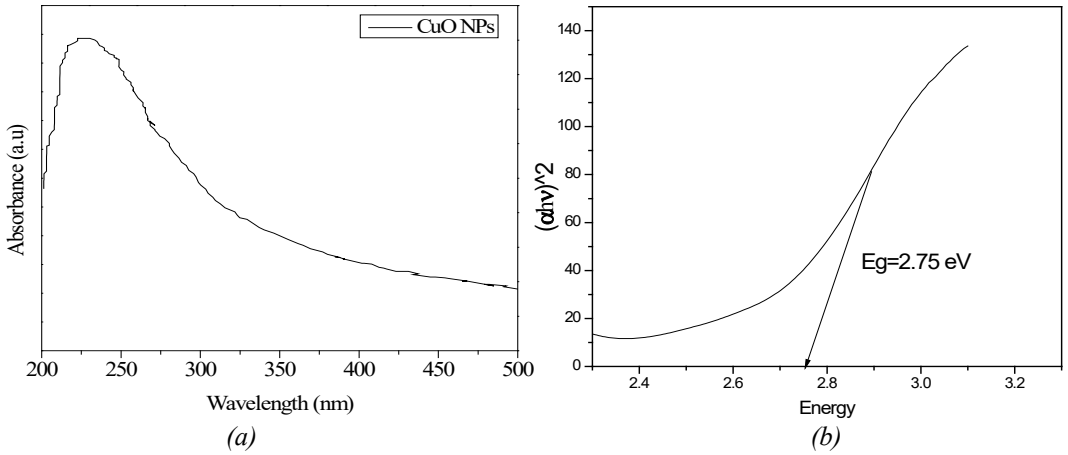

Fig. 6. (a-b). a) Ultraviolet-visible spectrum of the green combustion method of copper oxide nanoparticle synthesis using neem seed extract; b) Tauc plot.

3.4. XPS spectra

Fig 7 demonstrates the XPS spectra of CuONPs. Fig 7(a) provides an overview of the CuONPs prepared using the green synthesis method. CuONPs Cu2p spectra are presented in Fig 7(b). The Cu^{2+} and Cu^{+} specimens' Cu2p3/2 peaks match the energies of the two principal peaks, which are at 932 eV and 935.4 eV. The GO C 1s spectra displayed in Fig 7(c) showed four significant peaks at 282.8 eV, 284.4 eV, 286.7 eV, and 290 eV respectively. These peaks show carbon that has undergone sp^2 hybridization as well as carbon that serves as carboxyl, hydroxyl, and epoxide groups, among other activities. Fig 7(d) displays an O1s binding energy of 529.5 eV, suggesting that the catalyst of the nanoparticle contains CuO. Such an interpretation is supported by the Cu 2p1/2 peak at 944.8 eV and 941.8 eV. Accordingly, these stand for Cu^{2+} and Cu^{+} species. The adsorption of

oxygen (O_2) and water (H_2O) molecules from the nearby atmosphere results in the binding energies of the last two peaks, which are at 531.7 eV and 532.5 eV, respectively [46]. According to our results, the sample contains notable amounts of copper and oxygen elements, which further revealed the superior quality and purity of the green combustion method of copper oxide nanoparticles [47].

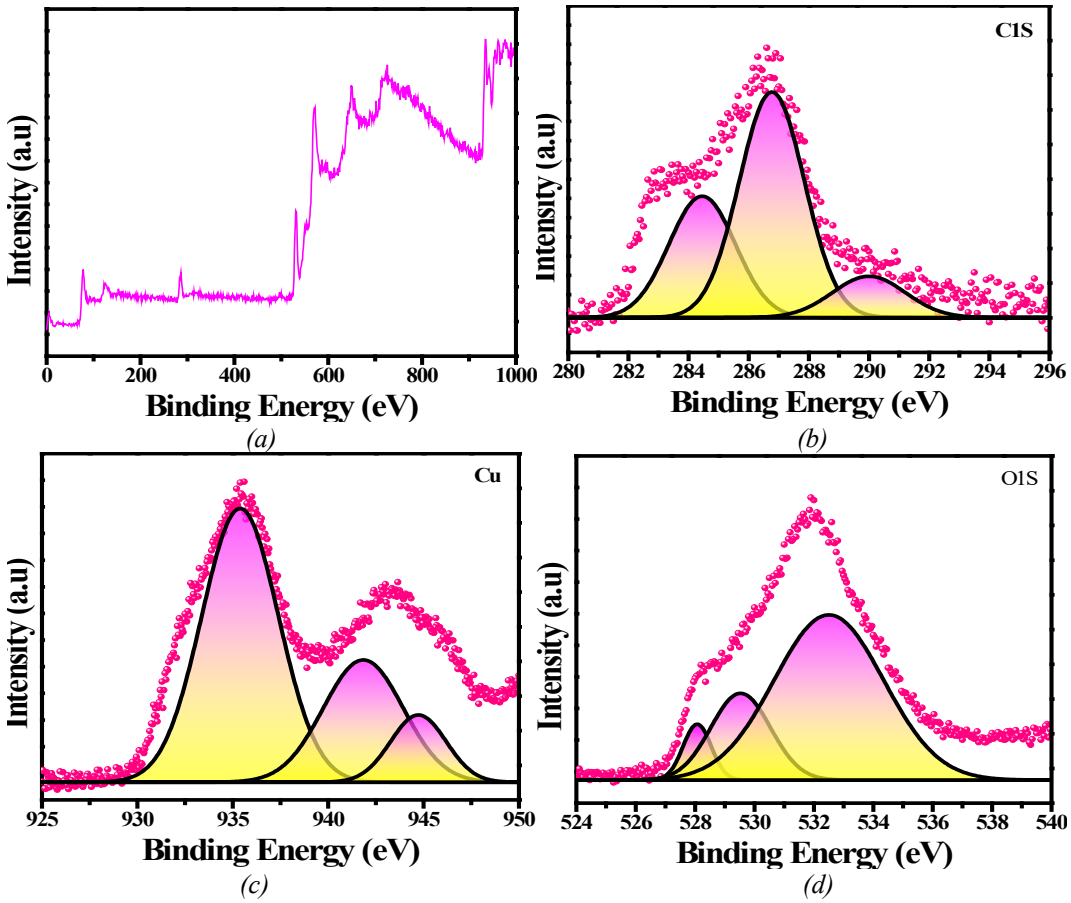

Fig. 7. (a-d) XPS spectrum of the green combustion synthesis of CuONPs from the seed extract of A. indica a) Survey; b) Cu; c) C1s; d) O1s.

3.5. Morphological analysis

SEM analysis was used to identify the CuONPs' morphological characteristics. CuONPs with spherical and undefined form morphologies are depicted in Fig 8(a-d). Extremely polydisperse nanoparticles are also present. Agglomerated CuONPs comprised many of the available samples. As a result, the SEM image verified the synthetic CuONPs characteristics [48]. The result aligns with previous research, in which a small proportion of the CuONPs exhibited amorphous forms, whereas the bulk existed in an aggregative state with minor deviations resulting from distinct chemical compositions [49]. As expected, agglomerations reduced as particle size grew, because increasing particle size has a linear effect on size. SEM of CuONPs showed the aggregation of particles is related to an attempt to reduce surface free energy. The surface possibilities are displayed with clarity, emphasizing the presence of CuONPs [50].

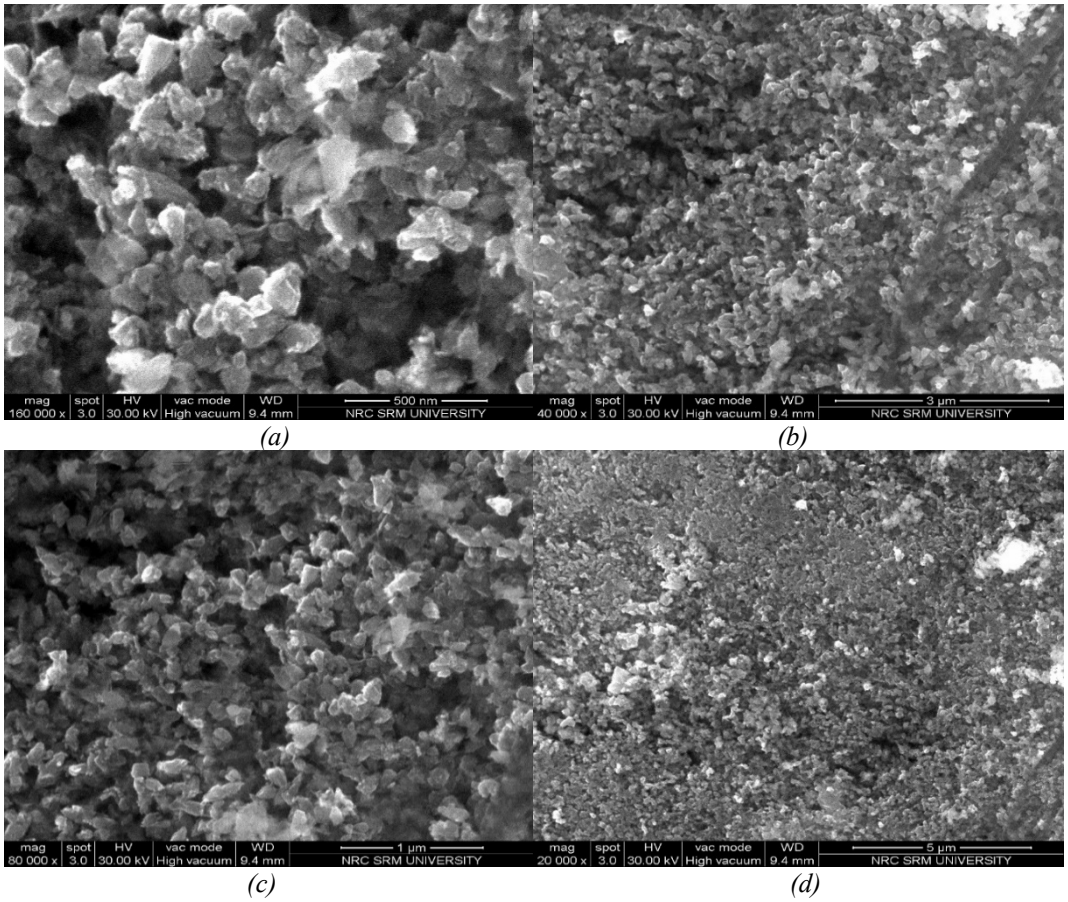

Fig. 8(a-d). SEM results of the green combustion synthesis of CuO nanoparticles at various magnifications a) 500 nm; b) 1 µm; c) 3 µm; d) 5 µm.

Fig 9(a-d) demonstrates the HRTEM image of the green synthesis method creating spherical CuONPs that were agglomerated and dispersed uniformly. Combustion produces spheres and undefined shapes because it raises temperatures to higher levels. In addition to magnetic interactions, low density, and weak interparticle forces - the heat created while burning and the resulting gas are other possible sources of agglomeration. The green synthesis method was used to form almost spherical CuONPs. Their diameter ranged from 5 to 20 nm, according to measurements. The mean diameter of the CuONPs was only 17.4 nm, as shown in Fig 9(a-d). CuONPs created in an environmentally friendly way have large specific surface areas, high dispersions, and small particle sizes which make them a valuable material for photodegradation investigations [51] that closely matches the images obtained from the SEM. Fig 9(d) shows the transmission electron microscopy image and the SAED pattern of CuONPs [52]. The polycrystalline character of the green combustion synthesis of CuO nanoparticles generated using the action of *A. indica* seed extract was demonstrated by SAED; displaying bright circular spots. The values of the matching interplanar spacing were determined to be 0.20 nm, 0.18 nm, 0.13 nm, and 0.11 nm, and the four distinct diffraction rings are visible. These values agree with the face-centered cubic copper crystalline planes 111, 200, 220, and 311 in their d spacing [53]. CuONPs with a particle size ranging from 10-190 nm, and with a roughly spherical shape was formed by Trichoderma asperellum, according to Alghuthaymi, Mousa A., et al. [54]. The analysis of particle size distributions was done using ImageJ software. The connections, spherical shape, and CuONPs aggregation are shown in Fig 9(e).

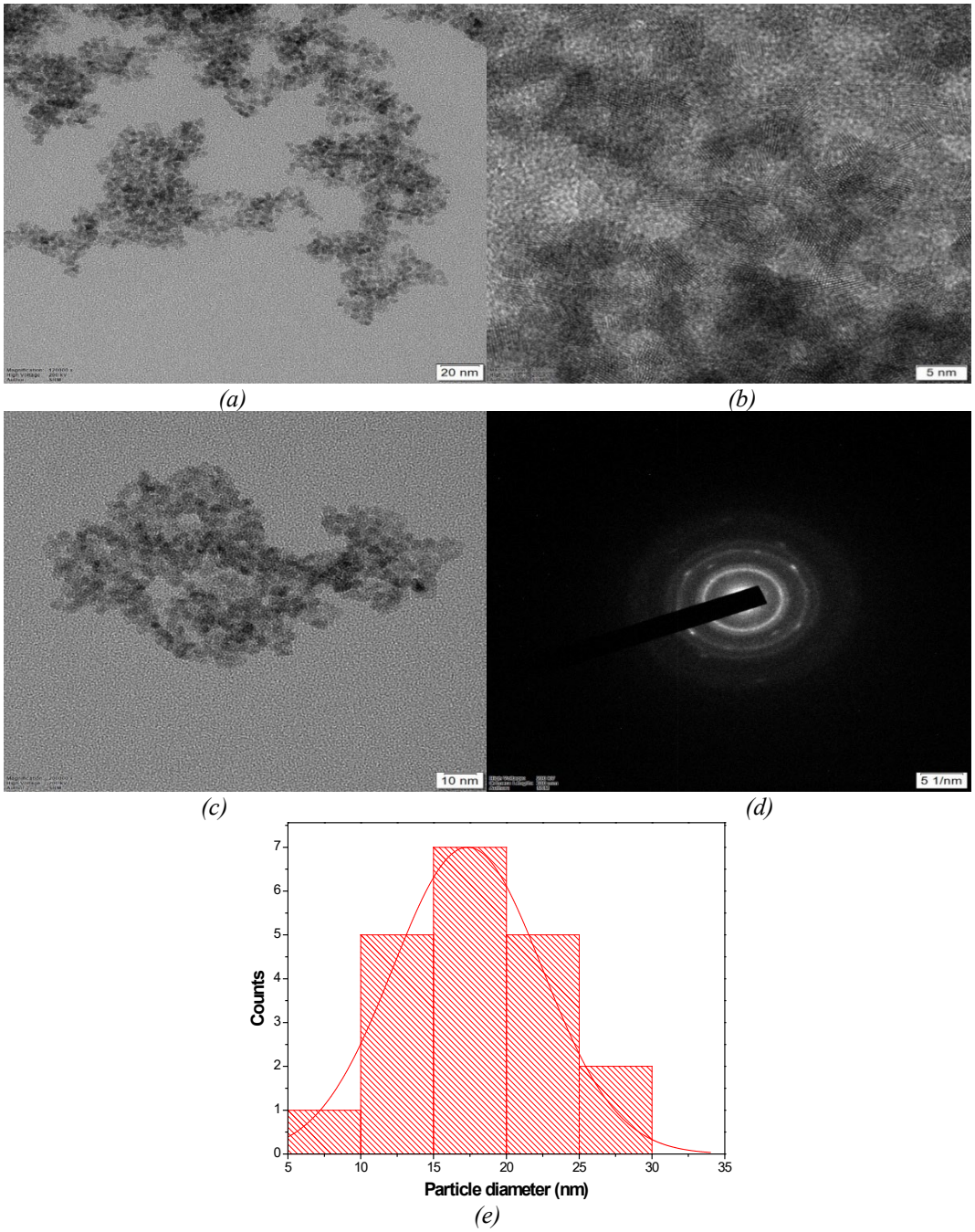

Fig. 9. (a-e). HRTEM results of the green synthesis of CuO nanoparticles at different magnifications (a) 20 nm, b) 10 nm, c) 5 nm, d) SAED pattern, and e) particle size distribution of HRTEM images.

3.6. Photocatalysis studies

CuONPs whole surface displayed the degradation of the dye rhodamine B in ultraviolet light. The greatest absorption wavelength at 552 nm is displayed in the ultraviolet-visible spectra of the degraded dye of RB in Fig 10(a), which displays the spectra across a time interval of 0 to 60 minutes. As the amount of time exposed to CuONPs increases, the absorbance intensities of RhB steadily decreases, suggesting a drop in RhB dye concentrations. Within 60 minutes of exposure, RhB dye undergoes a considerable 85% degradation. Neither the colour nor the concentration of the RhB dye varied when the reaction was performed for an hour in the dark. Fig 10(b) demonstrates the amount of RhB dye degradation in the formation of CuONPs as a function of irradiation time.

The longer the exposure period, the lower the relative RhB dye concentration. A generic Langmuir-Hinshelwood mechanism (4) is consistent with the apparent first-order kinetics of the RhB degrading reaction [55] Fig 10(c)

$$ln\left(\frac{C_0}{C_t}\right) = kt \tag{4}$$

In Rh-B dye photodegradation, 'k' denotes the pseudo-1st-order rate constant (min-1).

Additional proof regression values (R_2) for CuONPs were used to determine the nano-composite systems which were significantly closer to unity (0.9194) and hence more appropriate for first-order kinetics. The photocatalysis process occurs in CuONPs upon exposure to ultraviolet light. Plotting a straight line against time and noting its slope as ln(C_0/C) gives rise to the apparent 1st-order rate constant Kapp (0.00624 min t-1).

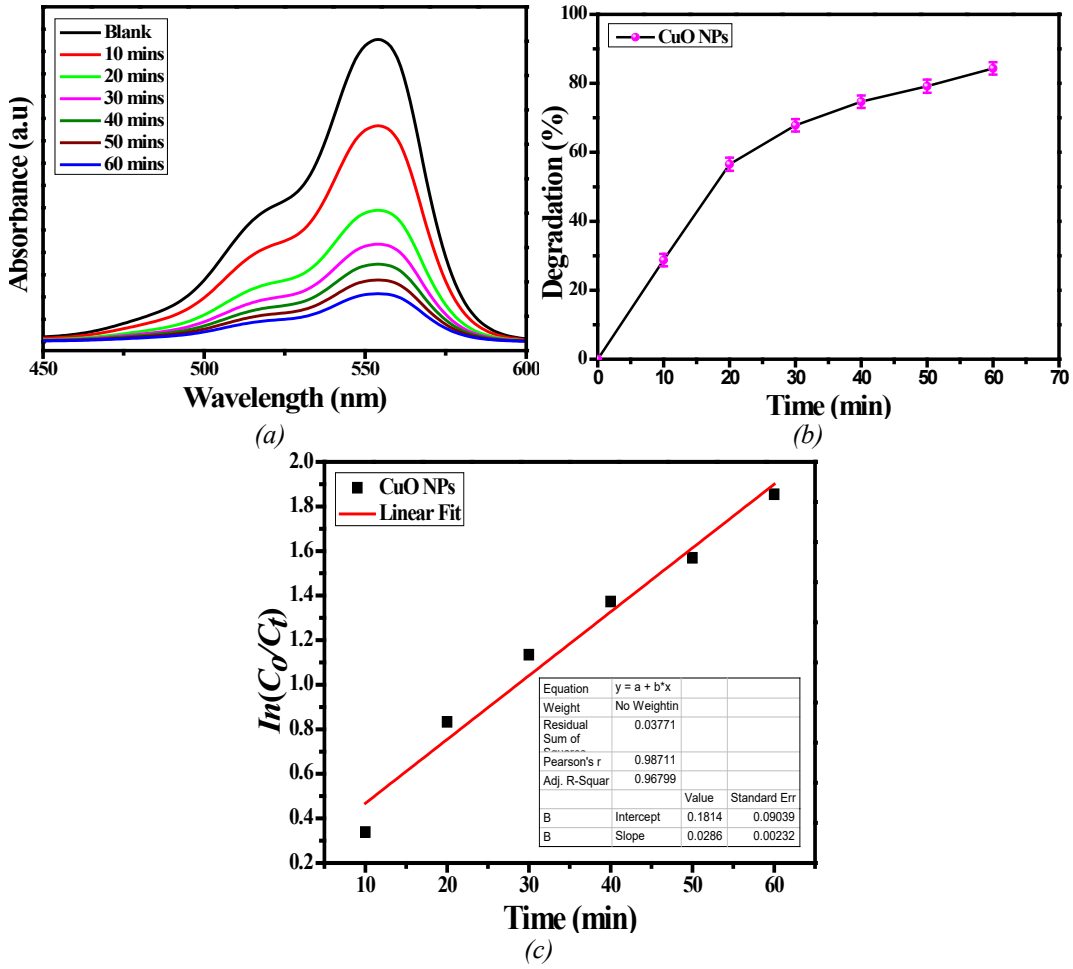

Fig. 10. (a-c). (a) Photocatalytic activity of prepared CuO nanoparticles for RhB dye solution under UV irradiation at 60 min; (b) RhB dye degradation percentage vs. irradiation time; (c) RhB dye degradation kinetics of the produced photocatalysts.

Fig 11 depicts the RhB dye's degradation over CuONPs. These processes may be caused by the successful separation of photogenerated e$^-$h+ pairs, which essentially show a vital character in RhB degradation [56]. The RhB degradation could proceed as follows:

$$CuO + hv \rightarrow CuO\ (e^- + h^+)$$
$$CuO + hv \rightarrow CuO\ (e^-) + CuO\ (h^+)$$

$$CuO\ (h^{+}) + H_2O + \rightarrow HO\bullet + H^{+}$$
$$CuO\ (e^{-}) + O_2 + \rightarrow O_2 -\bullet$$
$$HO\bullet + Rh\text{-}B \rightarrow CO_2 + H_2O$$
$$O_2 -\bullet + H + \rightarrow HOO\bullet$$
$$HOO\bullet + HOO\bullet \rightarrow H_2O_2 + O_2$$
$$O_2 -\bullet + Rh\text{-}B \rightarrow H_2O + CO_2$$
$$HOO\bullet + Rh\text{-}B \rightarrow H_2O + CO_2$$

The mechanism underlying CuONP's photocatalytic activity can be seen in Fig 11. When electrons from the VB are excited into the CB by a light source, a hole forms in the VB. The reaction sample's H_2O molecules are oxidised by the photocatalyst holes into more reactive OH radicals. Reduced oxygen molecules become O_2 radicals, and because of the excited electrons in the CB, decreased H_2O_2 molecules turn into OH radicals. CuONP can generate hydroxyl and oxide radicals, which can cause the dye to undergo oxidative degradation into carbon dioxide, water, and other mineralisation products [57]. Bio-synthesis of CuONP has a greater surface area, which makes their capacity for photocatalysis. The study also found that, in comparison to the other photocatalysts (Table 1), the current method produced appreciable dye degradation.

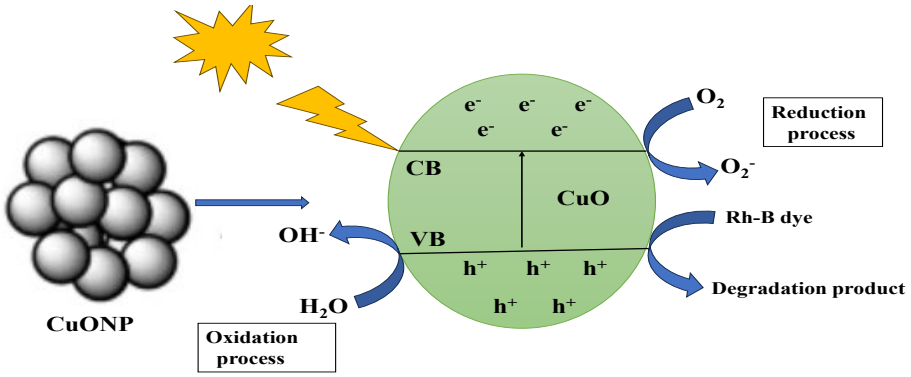

Fig. 11. The Rh-B dye photodegradation mechanism of the green synthesis of CuO nanoparticles.

After 60 minutes of UV light irradiation, RhB CuONPs' demonstrated a consistent decrease in absorbance intensity at λ_{max} = 552 nm, indicating an 85% degradation efficacy against RhB. Fig 10(a) represents the samples' efficiency of photocatalytic degradation [58]. CuONPs' increased efficiency could be attributed to the following factors: (1) a longer charge carrier lifetime and efficient separation of the photogenerated charge carriers; (2) a high concentration of defects or oxygen vacancies that serve as photogenerated electron trapping sites. Moreover, these oxygen vacancies can facilitate the absorption of O_2, which gets converted into superoxide radicals (O_2). OH^- and H_2O_2 radicals are produced by these superoxide radicals, which degrade to organic colour molecules [59].

Table 1. Comparison study for photocatalytic activity: previous work and current work.

Method	catalyst	dye	Concentration	reduction time	K (min^{-1})	degradation rate %	Ref
Green synthesis	CuO NPs	RhB	1 mg/L	105	-	78	[60]
Green synthesis	CuOSA/ GO	RhB	10 mg/L, c	60	0.007	36	[61]
Green synthesis	CuO NPs	RhB	20 mg/L	60	0.91	85	Present study

3.7. Stability studies

Centrifugation was used to remove the CuONPs from the solution following the completion of the initial trial in this work. They were washed five times through ethanol and distilled water, dried in an oven at 80 °C, and then employed as photocatalysts in five trials. The stability was evaluated by recycling the photocatalysts with an equivalent volume of new RhB after each run. Following every run, the same amount of fresh RhB was added to test the photocatalyst's stability. The stability and photocatalytic recyclability of the resultant CuONPs' were examined after the activity was carried out five times. The five CuONPs' cycles were compared in Fig 10(b), based on removal efficiency (%) and reaction time (minute). Centrifugation and precipitation can be used to recover the freshly generated colours, allowing the catalyst to be recycled after each cycle. Numerous investigations have shown that CuONPs is both efficient and recyclable when exposed to light. Catalyst efficiency was decreased by 10% after five cycles. After five cycles, the photocatalytic activity did not change. The first, second, third, fourth, and fifth runs had deterioration rates of 85%, 83.54%, 79.98%, 79.96%, and 79.94%, respectively. The generated CuONPs' stability and photocatalytic recyclability were examined after the activity was carried out five times. For each of the five CuO nanoparticle cycles, a comparison of the removal efficiency and reaction time was determined. The CuONPs' photo degradation efficiency under solar radiation was sustained at 79.94% following five cycles. This `low decreased efficiency showed that the catalyst is stable and making it appropriate for the catalytic breakdown of organic pollutants in wastewater clean-up [62]. Furthermore, for sufficient dye degradation after the first run, a longer incubation period was required. The activity of photocatalytic degradation decreased slightly after five cycles of reusability, which may have been caused by overcrowding or a decline in photocatalytic activity from frequent use. These findings also imply that the method might be applied in real-time wastewater treatment scenarios. After five consecutive cycles, the photocatalyst in the CuONPs' has demonstrated exceptional performance and consistent catalytic activity [63].

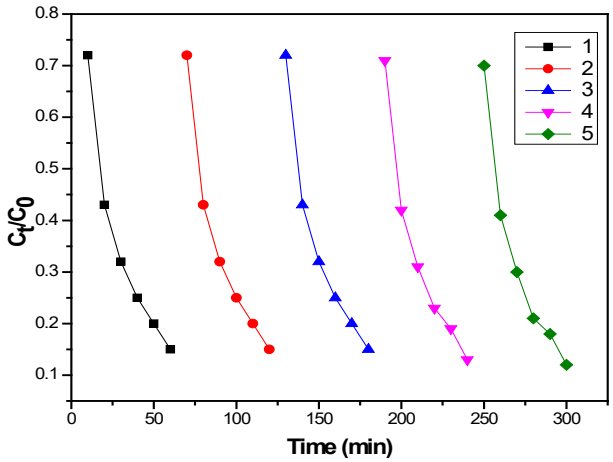

Fig. 12. Cycling procedures degrade RhB dye photocatalytically over CuONPs' that are exposed to UV light.

At 60 minutes, the maximal photodegradation of RhB for CuO photocatalysts was 85%, 83.54%, 79.98%, 79.96%, and 79.94%, respectively. RhB degradation increased with increasing irradiation time, as seen in Fig 12. Due to the abundance of active sites, it was discovered that the degradation rate of CuONPs' was high during the first 60 minutes of effective irradiation, reaching 85%, 83.54%, 79.98%, 79.96%, and 79.94% for CuONPs', respectively. Later, the rate of degradation progressively decreased. This suggests that the repulsion of the dye particles from the catalyst surface will cause the rate of degradation to slow down after 60 minutes.

3.8. Anticancer activity of copper oxide nanoparticles with neem seed extract

The basic characteristics of cancer include the unchecked growth and multiplication of cancer cells, which are crucial for the formation of tumour and the spread of cancer. As a result, many chemo-preventive and therapeutic drugs can limit the proliferation of tumour cells. Neem seed extracts retards the progression of the cell cycle, which prevents tumour cells from growing and multiplying. HeLa cervical tumour cells are inhibited for their growth by neem seed, and NLE prevents prostate cancer cells from proliferating [64]. A human renal adenocarcinoma cell line was used to test the cytotoxicity of CuO nanoparticles using the MTT assay. The outcomes were contrasted with those of cyclophosphamide, which is the gold standard. The seed extract from *A. indica* was used in our study and the effects of dosage on the toxicity of CuONPs' against cancer cell types were shown in Fig 13. We used concentrations of CuONPs' at 5, 10, 25, 50, and 100 mg to investigate the effect on anticancer activities. As the CuONPs' concentration increased, the anticancer activity also increased. For this reason, the concentration of CuONPs' works as well as the anticancer drugs. CuO nanoparticles weighing 5 mg were evaluated for their half-lives in multiple cancer cell types. The highest inhibiting doses were 50 mg and 100 mg. Treating human renal adenocarcinoma cancer cells with CuONPs' gave no appreciable results. It was demonstrated that in human renal adenocarcinoma cancer cells, 50 g and 100 g were required to induce 50% cell death [65]. Metal nanoparticles enhanced the anticancer impact of green-produced CuONPs'; this effect may have been caused by the form and aggregation of the nanoparticles. The current investigation demonstrated that CuONPs' will function as effective drug carriers in biological contexts.

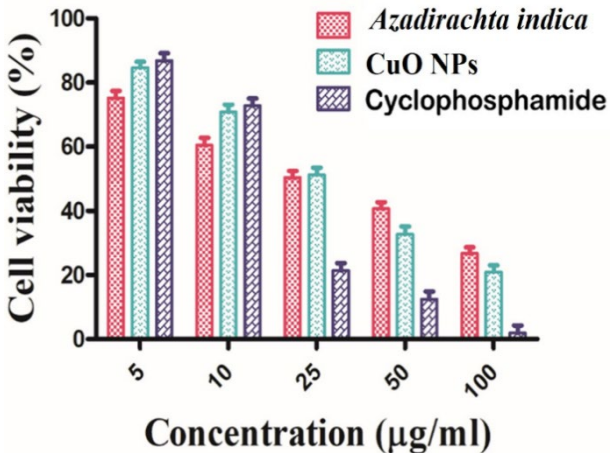

Fig. 13. Anticancer activity of the green combustion synthesis of copper oxide nanoparticles from neem seed extract.

4. Conclusions

Simple, affordable, and environmentally friendly CuONPs' were created using *A. indica* seed extract. While the CuONPs' were produced, the biometabolites found in *A. indica* served as stabilising and reducing agents. The synthesis of CuONPs' in XRD showed apprciable crystalline quality, with a mean crystallite size of 12 nm. The X-ray diffractometry examination verified that CuONPs' were in the fcc cubic phase.

The biosynthesis of CuO nanoparticle's FTIR spectra revealed a prominent and strong absorption band at 532 cm^{-1}. The CuO nanoparticle's optical band gaps were 2.75 eV in UV-vis, and their maximum absorption wavelength was 232 nm. In XPS, the CuO nanoparticles contains notable amounts of copper and oxygen elements, which further revealed the superior quality and purity of the green synthesis of copper oxide nanoparticles by combustion method.

The spherical and undefined shape of the CuO NPs was evaluated using HRTEM and SEM, and their mean particle size was 17.4 nm. Strong anticancer activity is shown even at high doses when evaluated against the human renal adenocarcinoma cancer cell line. It is an excellent source of anti-cancer properties. To conduct the photocatalytic experiment, RhB dye was degraded over green-produced CuO nanoparticles while exposed to UV light. Over 60 minutes, RhB dye significantly degraded by 85% over the CuO NPs. The rate constant of the RhB dye degradation reaction, k (0.9194 min-1), was found to be consistent with the first-order kinetic mechanism. The results of our meticulous, skilled, and original study demonstrated that the green method of synthesis of copper oxide nanoparticles makes it an excellent choice for pollution control management.

References

[1] O. Gohar, M. Z. Khan, I. Bibi, N. Bashir, U. Tariq, M. Bakhtiar, et al., Mater Des, 241, 112930, (2024); https://doi.org/10.1016/j.matdes.2024.112930

[2] M. A. Al-Nuaim, A. A. Alwasiti, Z. Y. Shnain, Chem Pap, 77(2), 677-701, (2023); https://doi.org/10.1007/s11696-022-02468-7

[3] S. Yadav, K. Shakya, A. Gupta, D. Singh, A. R. Chandran, V. A. Varayil Aanappalli, et al., Environ Sci Pollut Res Int, 30(28), 71912-32, (2023); https://doi.org/10.1007/s11356-023-27485-1

[4] M. Elangovan, P. D. Babu, T. Balaji, Int Res J Adv Sci Hub, 3(9S), 23-8, (2021); https://doi.org/10.47392/irjash.2021.244

[5] W. Strielkowski, L. Civín, E. Tarkhanova, M. Tvaronavičienė, Y. Petrenko, Energies, 14(24), 8240, (2021); https://doi.org/10.3390/en14248240

[6] R. Botella, W. Cao, J. Celis, J. Fernández-Catalá, R. Greco, L. Lu, et al., J Phys Condens Matter, 36(14), 141501, (2024); https://doi.org/10.1088/1361-648X/ad14c8

[7] M. A. Ahmed, A. A. Mohamed, RSC Adv, 13(1), 421-39, (2023); https://doi.org/10.1039/D2RA07225D

[8] S. H. Khan, Green Mater Wastewater Treat, 13-46, (2020); https://doi.org/10.1007/978-3-030-17724-9_2

[9] M. Sen, M. Mukherjee, editors, Bioinspired and Green Synthesis of Nanostructures: A Sustainable Approach, John Wiley & Sons, (2023); https://doi.org/10.1002/9781394174928

[10] M. B. Tahir, M. Sohaib, M. Sagir, M. Rafique, Encycl Smart Mater, 578, (2022); https://doi.org/10.1016/B978-0-12-815732-9.00006-1

[11] K. K. Kefeni, B. B. Mamba, Sustain Mater Technol, 23, (2020); https://doi.org/10.1016/j.susmat.2019.e00140

[12] G. Anandhi, M. Iyapparaja, RSC Adv, 14(13), 9003-19, (2024); https://doi.org/10.1039/D4RA00711E

[13] T. Adane, A. T. Adugna, E. Alemayehu, J Chem, 2021, 5314404, (2021); https://doi.org/10.1155/2021/5314404

[14] P. Chowdhury, K. S. Anantharaju, K. Keshavamurthy, S. L. Rokhum, J Chem, 2023, 9780955, (2023); https://doi.org/10.1155/2023/9780955

[15] Sarkodie, J. Amesimeku, C. Frimpong, E. K. Howard, Q. Feng, Z. Xu, Chemosphere, 313, 137654, (2023); https://doi.org/10.1016/j.chemosphere.2022.137654

[16] Haleem, M. Ullah, A. Shah, M. Farooq, T. Saeed, I. Ullah, et al., Water, 16(11), 1588, (2024); https://doi.org/10.3390/w16111588

[17] J. J. Samuel, F. K. Yam, Mater Res Express, 7(1), 015051, (2020); https://doi.org/10.1088/2053-1591/ab6409

[18] P. Sivaguru, S. Balakumar, Rasayan J Chem, 17(3), 905-15, (2024); https://doi.org/10.31788/RJC.2024.1738870

[19] K. A. Khan, A. Shah, J. Nisar, A. Haleem, I. Shah, Molecules, 28(12), 4600, (2023); https://doi.org/10.3390/molecules28124600

[20] Y. Ge, H. Luo, J. Huang, Z. Zhang, Opt Mater., 115, 111058, (2021); https://doi.org/10.1016/j.optmat.2021.111058

[21] H. A. A. Jamjoum, K. Umar, R. Adnan, M. R. Razali, M. N. Mohamad Ibrahim, Front Chem, 9, 752276, (2021); https://doi.org/10.3389/fchem.2021.752276

[22] K. Lakshmi, V. RajaRajeswari, R. R. Muthu Chudarkodi, Sensors, 3, 5, (2023).

[23] N. Chakraborty, J. Banerjee, P. Chakraborty, A. Banerjee, S. Chanda, K. Ray, et al., Green Chem Lett Rev, 15(1), 187-215, (2022); https://doi.org/10.1080/17518253.2022.2025916

[24] H. Mondal, Orient J Chem, 40(2), (2024); https://doi.org/10.13005/ojc/400208

[25] N. T. T. Nguyen, L. M. Nguyen, T. T. T. Nguyen, T. T. Nguyen, D. T. C. Nguyen, T. V. Tran, Environ Chem Lett, 20(4), 2531-71, (2022); https://doi.org/10.1007/s10311-022-01398-w

[26] S. A. Akintelu, A. S. Folorunso, F. A. Folorunso, A. K. Oyebamiji, Heliyon, 6(7), e04508, (2020); https://doi.org/10.1016/j.heliyon.2020.e04508

[27] M. Omran, H. A. Al-Aoh, K. Albalawi, F. M. Saleh, Y. F. Alanazi, H. S. Al-Shehri, et al., Journal of Drug Delivery Science and Technology, 77, 103811, (2022); https://doi.org/10.1016/j.jddst.2022.103811

[28] S. Aroob, S. A. Carabineiro, M. B. Taj, I. Bibi, A. Raheel, T. Javed, et al., Catalysts, 13(3), 502, (2023); https://doi.org/10.3390/catal13030502

[29] W. W. Andualem, F. K. Sabir, E. T. Mohammed, H. H. Belay, B. A. Gonfa, Journal of Nanotechnology, 2020, 2932434, (2020); https://doi.org/10.1155/2020/2932434

[30] Saloki, S. J. Daharwal, Asian Journal of Pharmaceutical and Clinical Research, 16(7), 172-176, (2023); https://doi.org/10.22159/ajpcr.2023.v16i7.47122

[31] K. Araya-Castro, T.C. Chao, B. Durán-Vinet, C. Cisternas, G. Ciudad, O. Rubilar, Nature Communications 9, 78, (2020); https://doi.org/10.3390/pr9010078

[32] A.B. Krishna, P. Prema, Nature Communications 27, 525, (2021).

[33] V. Selvanathan, M. Aminuzzaman, L.H. Tey, S.A. Razali, K. Althubeiti, H.I. Alkhammash, et al., Nature Communications 14, 6379, (2021); https://doi.org/10.3390/ma14216379

[34] Dhaka, S.C. Mali, S. Sharma, R. Trivedi, Nature Communications 101108, (2023); https://doi.org/10.1016/j.rechem.2023.101108

[35] M. Kumar, V. Pratap, A.K. Nigam, B.K. Sinha, M. Kumar, J.K.G. Singh, Nature Communications 65, 57, (2021); https://doi.org/10.37398/JSR.2021.650308

[36] U.U. Bhamare, Y.S. Mali, A.Z. Shaikh, Nature Communications 12, 245, (2020).

[37] M. Devaraji, P.V. Thanikachalam, K. Elumalai, Nature Communications (2024).

[38] Bhardwaj, P. Singh, A. Kumar, S. Kumar, V. Budhwar, Nature Communications 10, 566, (2020); https://doi.org/10.34172/apb.2020.067

[39] Dejene, R.F. Bogale, L. Yadeta, K.M. Gendo, G. Kenasa, A.L. Berhanu, Nature Communications 8, 101569, (2024); https://doi.org/10.1016/j.rechem.2024.101569

[40] Chauhan, R. Kumar, N. Thakur, M. Singh, K. Kumar, Nature Communications 6, 100199, (2024); https://doi.org/10.1016/j.hybadv.2024.100199

[41] Teklu, S.K. Kadiri, S. Vidavalur, Nature Communications 6, 101152, (2023); https://doi.org/10.1016/j.rechem.2023.101152

[42] J. Fu, X. Liu, L. Liu, H. Meng, X. Wang, Nature Communications 752, 012060, (2020).

[43] A.N. Labaran, Z.U. Zango, G. Tailor, A. Alsadig, F. Usman, M.T. Mukhtar, et al., Nature Communications 14, 5589, (2024); https://doi.org/10.1038/s41598-024-56052-y

[44] G.S.R.E.P. Sabeena, S. Rajaduraipandian, E. Pushpalakshmi, H.A. Alhadlaq, R. Mohan, G. Annadurai, et al., Nature Communications 34, 102092, (2022); https://doi.org/10.1016/j.jksus.2022.102092

[45] Atri, M. Echabaane, A. Bouzidi, I. Harabi, B.M. Soucase, R.B. Chaâbane, Nature Communications 9, e14345, (2023); https://doi.org/10.1016/j.heliyon.2023.e14345

[46] K. Chung, J. Bang, A. Thacharon, H.Y. Song, S.H. Kang, W.S. Jang, et al., Nature Communications 17, 285, (2022); https://doi.org/10.1038/s41565-021-01070-4

[47] M.A. Khan, N. Nayan, M.K. Ahmad, C.F. Soon, Nature Communications 10, 1298, (2020); https://doi.org/10.3390/nano10071298

[48] G. Anbalagan, B. Subramanian, V. Suresh, P. Sivaperumal, Nature Communications 16, e5643, (2024); https://doi.org/10.7759/cureus.5643

[49] W. Kiciński, S. Dyjak, Nature Communications 168, 748, (2020); https://doi.org/10.1016/j.carbon.2020.07.014

[50] J. Borgatta, Y. Shen, C. Tamez, C. Green, J.K. Hedlund Orbeck, M.S. Cahill, et al., Nature Communications 71, 9644, (2023); https://doi.org/10.1021/acs.jafc.2c07543

[51] K. Ganesan, V.K. Jothi, A. Natarajan, A. Rajaram, S. Ravichandran, S. Ramalingam, Nature Communications 13, 6802, (2020); https://doi.org/10.1016/j.arabjc.2020.06.019

[52] L. Ragunath, J. Suresh, M. Sankaran, R.S. Kumar, A.I. Almansour, N. Arumugam, Nature Communications 14, 2660, (2021); https://doi.org/10.31788/RJC.2021.1446512

[53] Z. Leng, D. Wu, Q. Yang, S. Zeng, W. Xia, Nature Communications 154, 33, (2018); https://doi.org/10.1016/j.ijleo.2017.10.036

[54] M.A. Alghuthaymi, K.A. Abd-Elsalam, H.M. AboDalam, F.K. Ahmed, M. Ravichandran, A. Kalia, et al., Nature Communications 8, 367, (2022); https://doi.org/10.3390/jof8040367

[55] N. Akram, J. Guo, W. Ma, Y. Guo, A. Hassan, J. Wang, Nature Communications 10, 1939, (2020); https://doi.org/10.1038/s41598-020-59053-9

[56] P. Raizada, V. Soni, A. Kumar, P. Singh, A.A.P. Khan, A.M. Asiri, et al., Nature Communications 7, 388, (2021); https://doi.org/10.1016/j.jmat.2021.02.009

[57] T.B. Mekonnen, Nature Communications 6, 115, (2022).

[58] M. Yaseen, T.A. Khan, A. Nazir, A.M. Asiri, S.B. Khan, Nature Communications 27, 5343, (2022); https://doi.org/10.3390/molecules27165343

[59] M. Singh, A. Garg, R. Shukla, N. Verma, M. Sharma, Oxygen-deficient photostable Cu_2O for enhanced visible light photocatalytic activity. Nanoscale 10(13), 6039-6050, (2018); https://doi.org/10.1039/C7NR08388B

[60] M. Jeevarathinam, I.V. Asharani, Synthesis of CuO, ZnO nanoparticles, and CuO-ZnO nanocomposite for enhanced photocatalytic degradation of Rhodamine B: A comparative study. Scientific Reports 14(1), 9718, (2024); https://doi.org/10.1038/s41598-024-60008-7

[61] S. Aroob, A. Shabbir, R. Mahmood, S. Ali, S. Naz, Journal of Environmental Chemical Engineering 9(4), 105590, (2021); https://doi.org/10.1016/j.jece.2021.105590

[62] P.G. Krishna, C.S. Kumar, M.S. Muthu, J. Bhattacharya, J. Sharma, Frontiers in Chemistry 10, 917831, (2022); https://doi.org/10.3389/fchem.2022.917831

[63] G. Ren, Y. Liu, Z. Zhang, X. Hou, Nanomaterials 11(7), 1804, (2021); https://doi.org/10.3390/nano11071804

[64] R.I. Mahmood, S. Aroob, A. Shabbir, A. Nazir, S. Naz, Scientific Reports 12(1), 16165, (2022); https://doi.org/10.1038/s41598-022-20360-y

[65] S. Naz, A. Gul, M. Zia, IET Nanobiotechnology 14(1), 1-13, (2020); https://doi.org/10.1049/iet-nbt.2019.0176